

## Supporting Information

### **The allosteric regulation mechanism on the catalytic activity of fructosyltransferase studied by molecular dynamics simulations**

Chaofan Yu<sup>1</sup>, Yanqi Liu<sup>1,2</sup>, Liang Fu<sup>2</sup>, Zhengyu Shu<sup>1</sup>, Mojie Duan<sup>2\*</sup>, Yi Zheng<sup>1,3\*</sup>

1 College of Life Science, Fujian Normal University, Fuzhou 350108, China

2 NMR and Molecular Sciences, School of Chemistry and Chemical Engineering, The State Key Laboratory of Refractories and Metallurgy Wuhan University of Science and Technology Wuhan 430081, China

3 National Joint Engineering Research Center of Industrial Microbiology and Fermentation Technology, College of Life Sciences, Fujian Normal University, Fuzhou 350108, China

#### **Corresponding authors**

Yi Zheng, [eyizheng@fjnu.edu.cn](mailto:eyizheng@fjnu.edu.cn)

Mojie Duan, [mduan@wust.edu.cn](mailto:mduan@wust.edu.cn); [mjduan@wipm.ac.cn](mailto:mjduan@wipm.ac.cn)

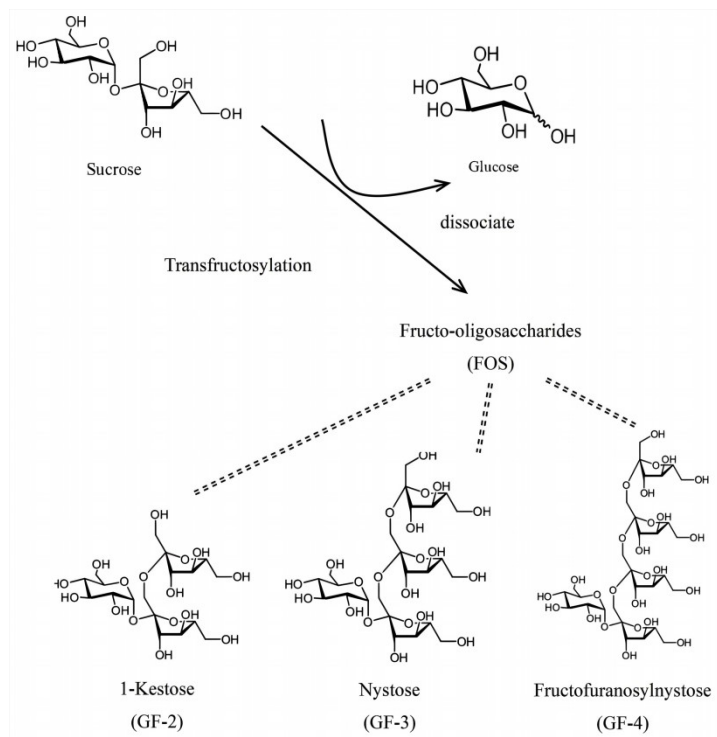


Figure S1. Mechanism of action of fructosyltransferases to generate oligofructose (FOS) by hydrolysis of sucrose as a substrate interacting with trans-fructosylation.

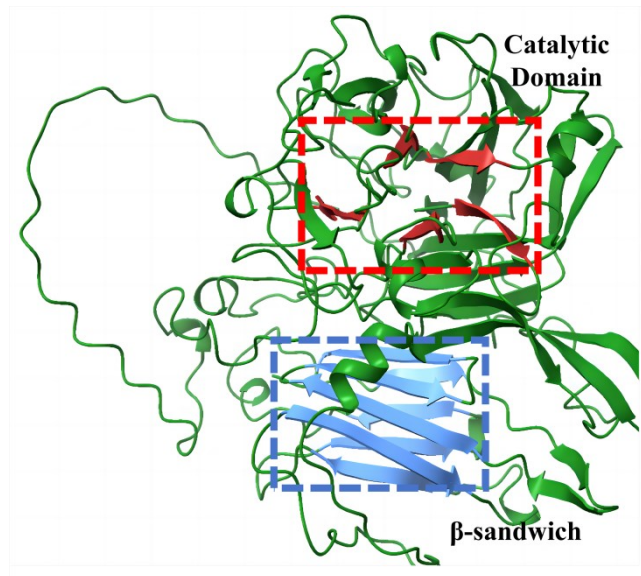


Figure S2. Schematic representation of the QU10-FTase structure.

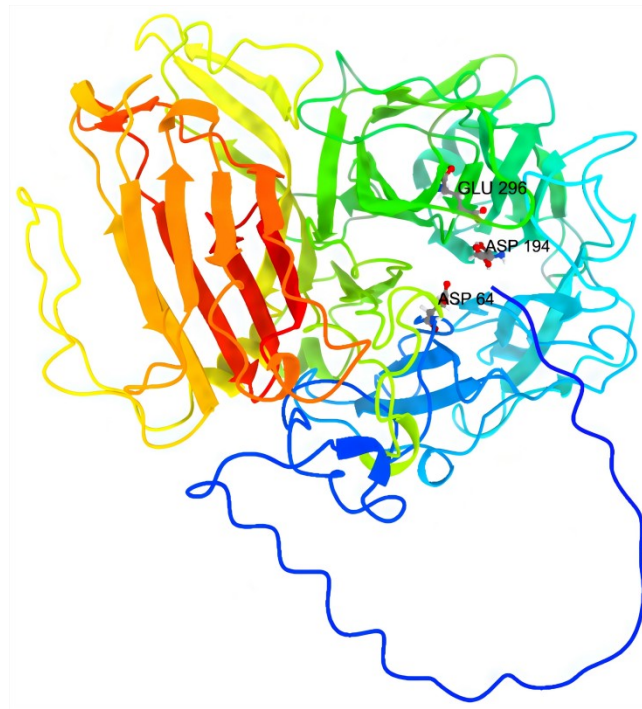


Figure S3. Schematic representation of the three key catalytic sites of QU10-FTase

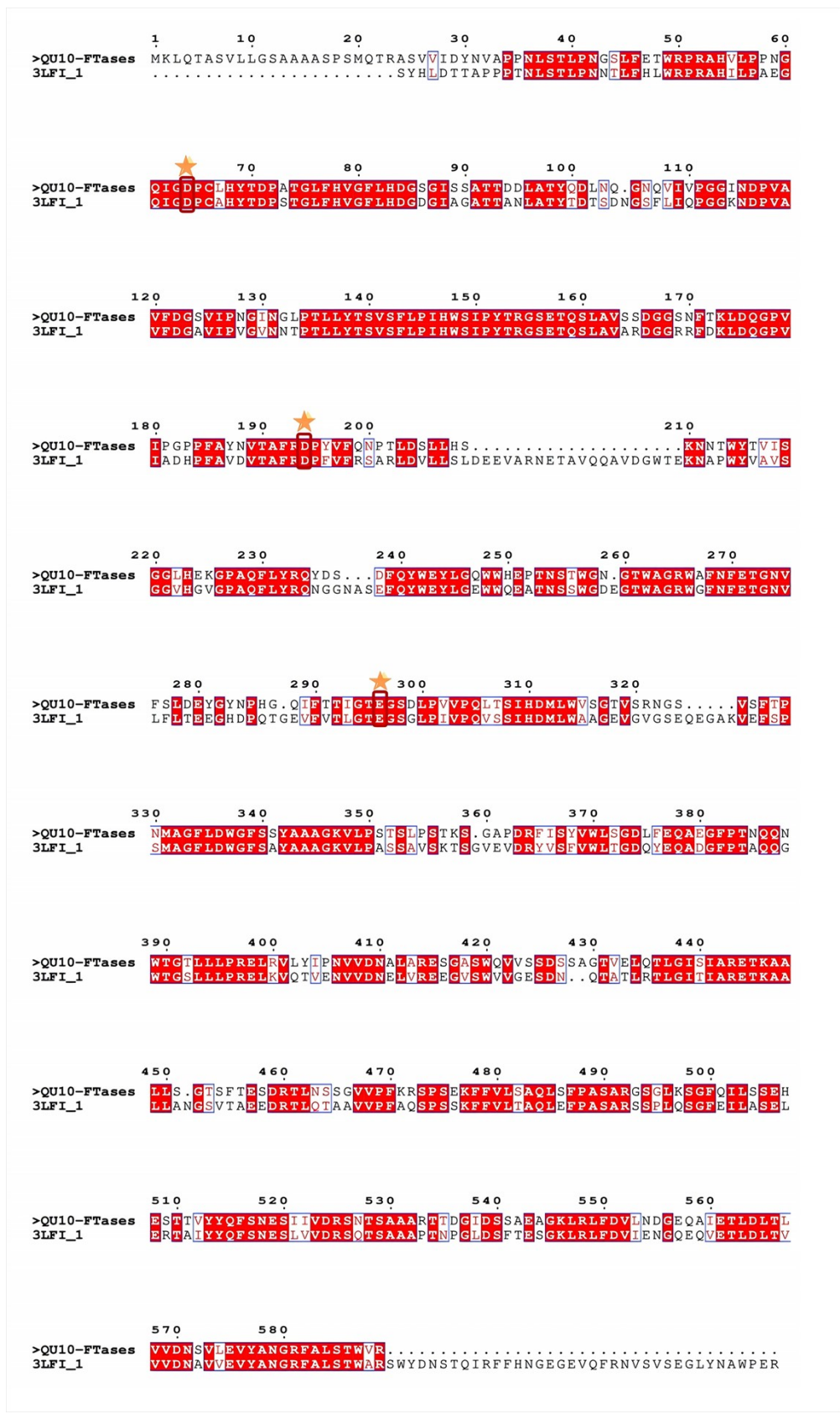


Figure S4. QU10-FTase sequence was compared with the FT sequence of *Aspergillus japonicus*.

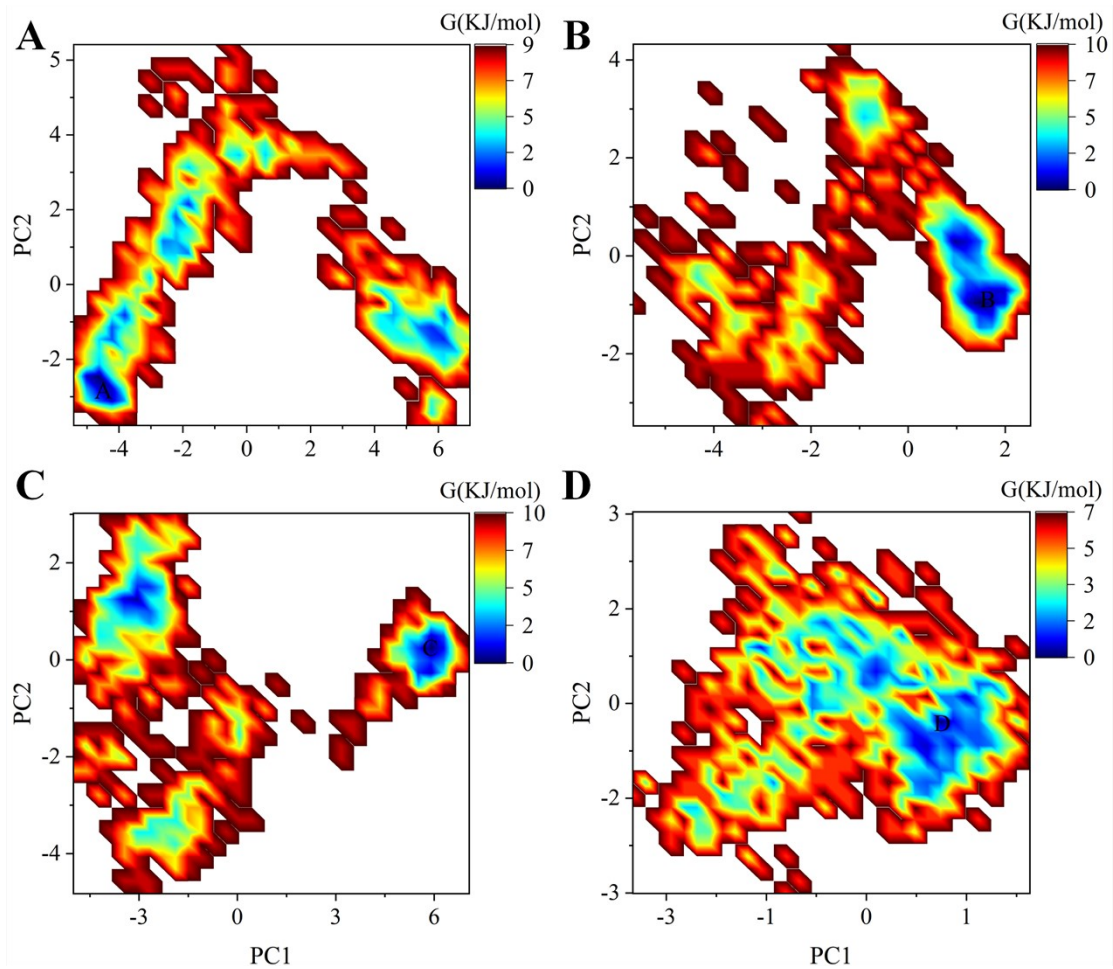


Figure S5. The principal component analysis of QU10-FTase related to the  $\text{Fe}_3\text{O}_4$  interfaces. The different panel figures are corresponding to the systems in Figure 2.

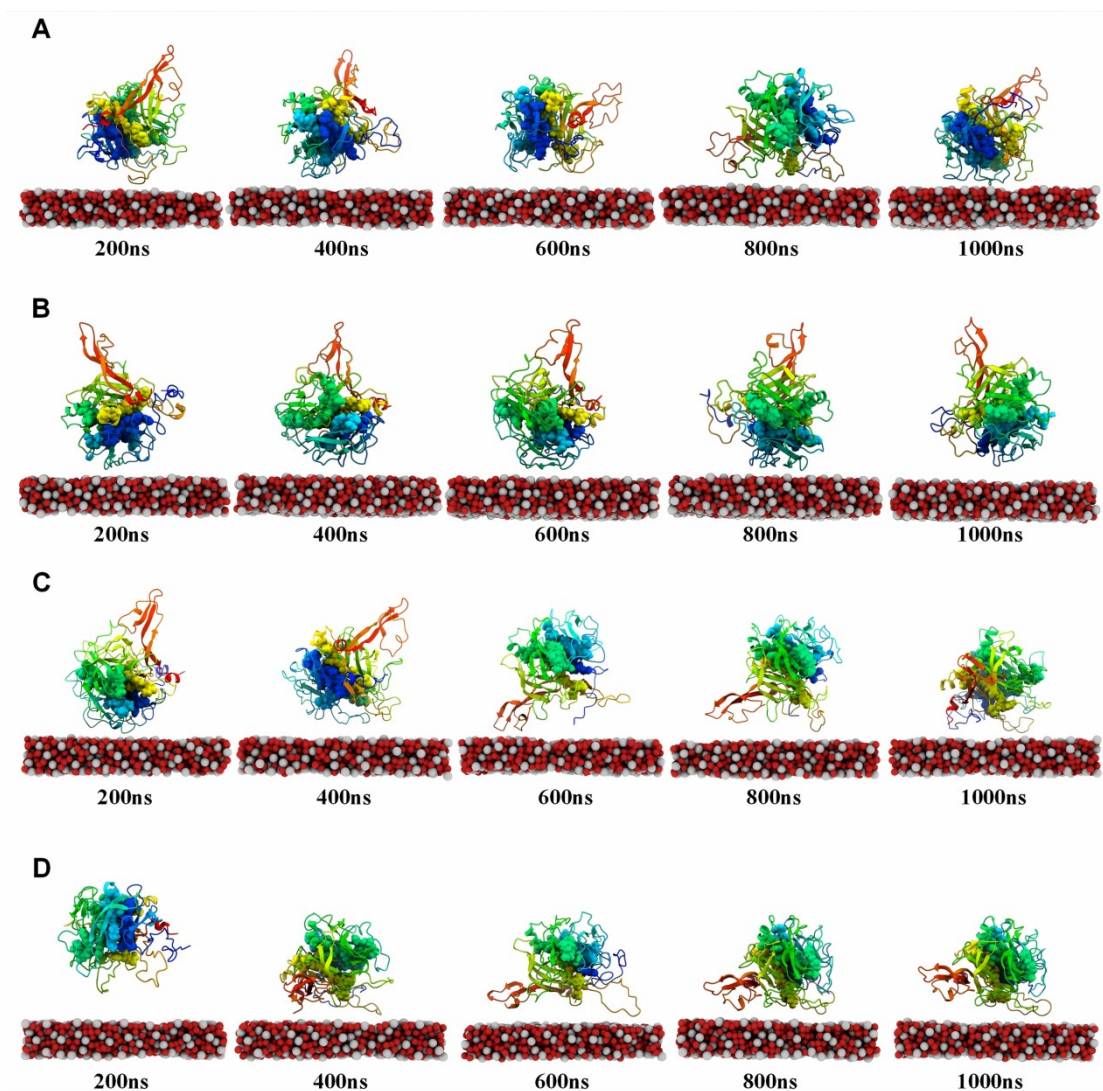


Figure S6. Conformational changes of QU10-FT in different postures at different time points. (A). The conformations of QU10-FT N&C away at 200ns, 400ns, 600ns, 800ns, and 1000ns, respectively. (B). QU10-FT N&C close conformations at 200ns, 400ns, 600ns, 800ns, and 1000ns, respectively. (C). QU10-FT pocket-C down conformations at 200ns, 400ns, 600ns, 800ns, and 1000ns, respectively. (D). The conformation of QU10-FT pocket-N down at 200ns, 400ns, 600ns, 800ns, and 1000ns, respectively.

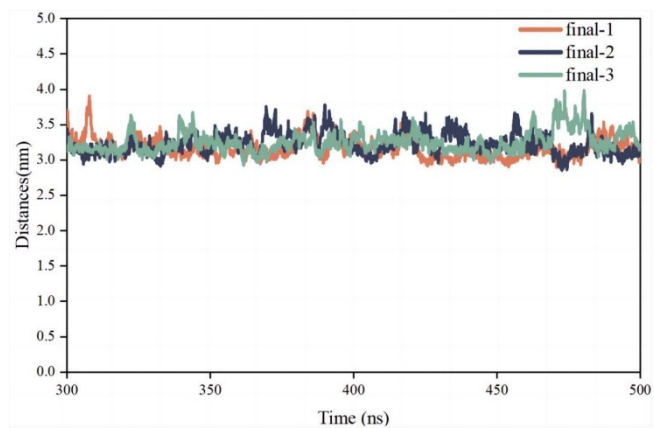


Figure S7. Distance between the center of mass of the  $\beta$ -strand and the  $\text{Fe}_3\text{O}_4$  surface of QU10-FT's 347-349 in three repetitions of the simulation as a function of time.



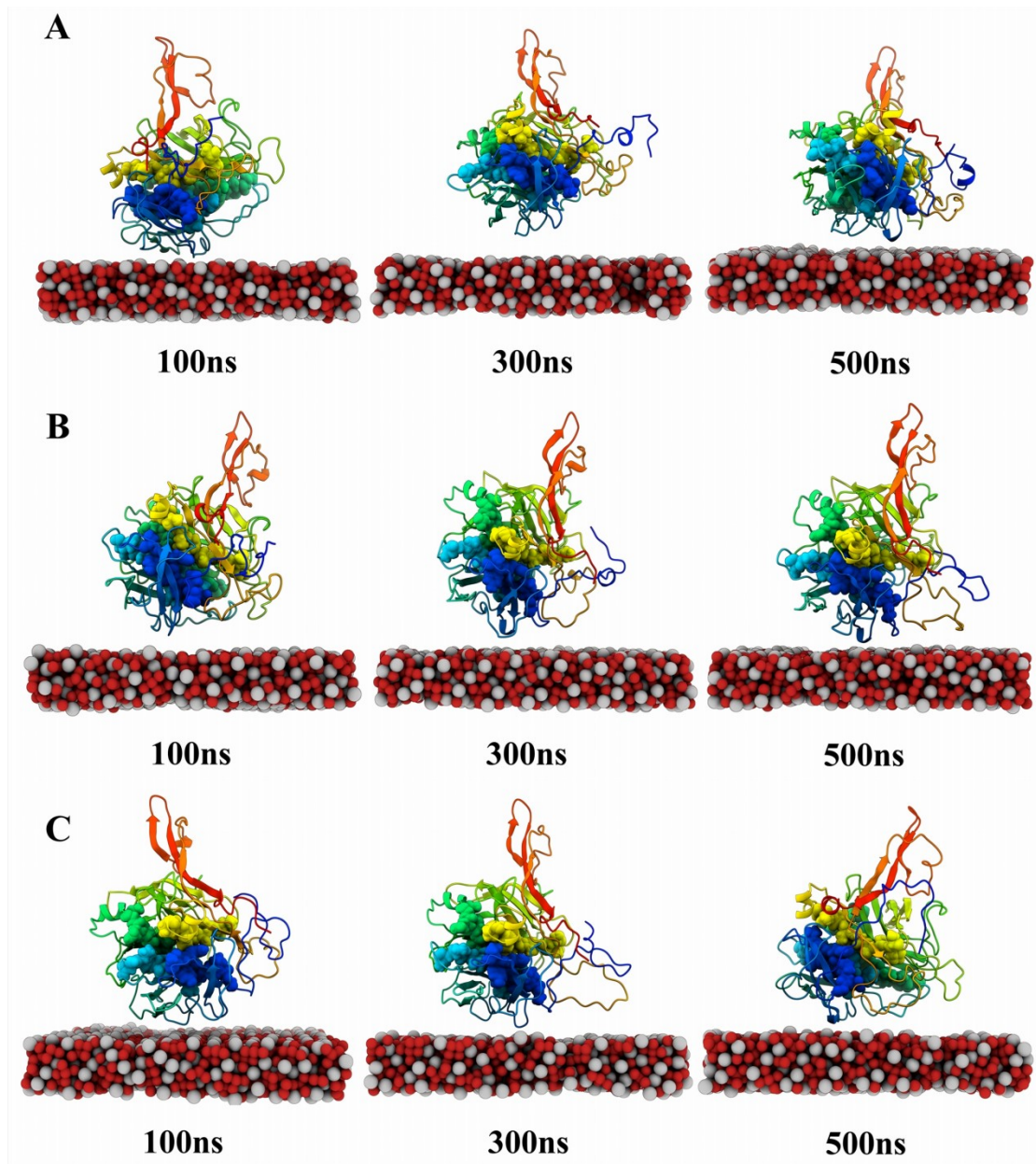


Figure S8. Conformational changes over time for three repetitions of the simulation.

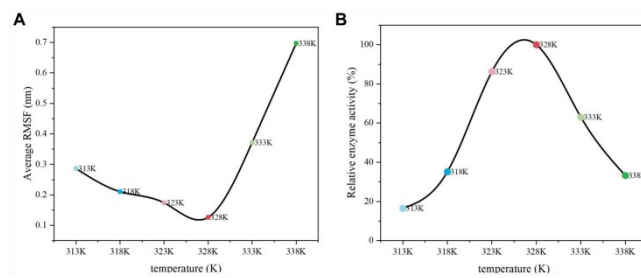


Figure S9. Relative enzyme activities of QU10-FTase and main chain RMSF curves under different temperature conditions.

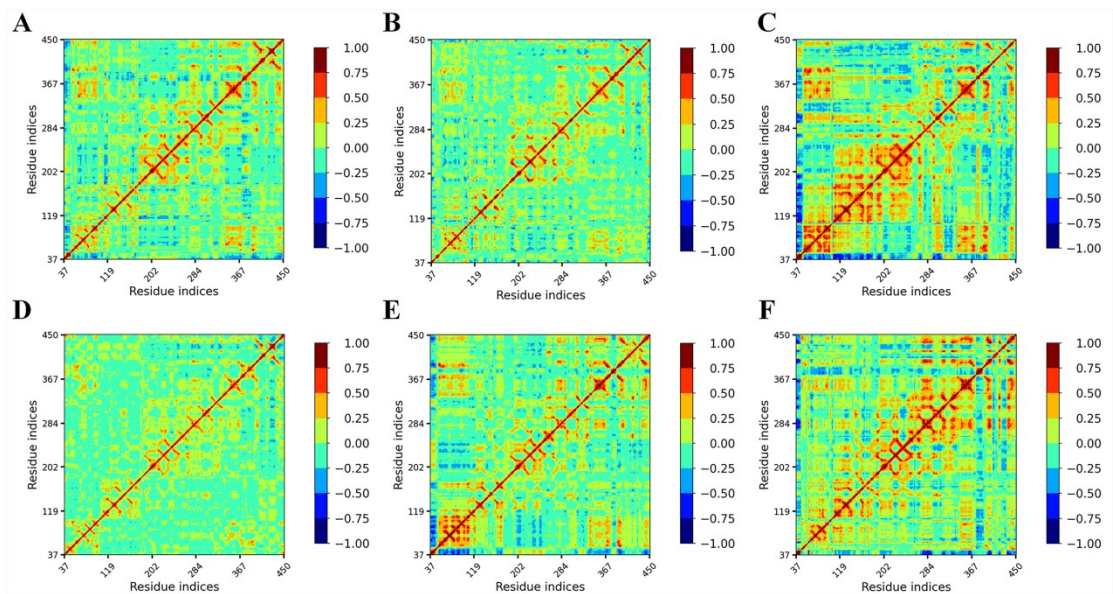


Figure S10. The dynamic correlation-coefficient (DCC) analysis of QU10-FTase under different temperature. (A) 313K; (B) 318K; (C) 323K; (D) 328K; (E) 333K; (F) 338K. The C $\alpha$  atoms of residues were utilized in the analysis.

**Table S1. LJ potential parameters and Morse bond parameters for Fe<sub>3</sub>O<sub>4</sub>**

ionic	$\epsilon$ (eV)	$\sigma$ (Å)	De(eV)	$\alpha$ (Å <sup>-1</sup> )	$r_0$ (Å)	q (C)
Fe <sup>2+</sup>	0.019584	3.900	3.637717	0.621504	2.350	1.251
Fe <sup>3+</sup>	0.000741	2.664	8.379944	0.518692	2.333	1.611
O <sup>2-</sup>	0.003400	3.627				

**Table S2. Contact sites and contact probabilities between QU10-FTase residues and Fe<sub>3</sub>O<sub>4</sub>.**

exposure probability	contact site
1%~20%	47A 59N 60G 101D 102L 103N 116D 131N 133L 144L 145P 146I 150I 151P 153T 155G 156S 165S 167G 169S 170N 174L 176Q 303V 304P 374D 377E 378Q 379A 381G 382F 383P 387Q
20%~40%	107Q 118V 143F 172T 173K 305Q 380E 385N 388N
40%~60%	61Q 83H 86S 110V 111P 113G 166D 384T
60%~80%	104Q 105G 117P
>80%	84D 85G 106N 112G 114I 175D 386Q